Journal of Medicinal Chemistry

Article

pubs.acs.org/jmc

Fluorescent Inhibitors as Tools To Characterize Enzymes: Case Study of the Lipid Kinase Phosphatidylinositol 4-Kinase IIIβ (PI4KB)

Jana Humpolickova,[†,§] Ivana Mejdrová,[†,‡,§] Marika Matousova,[†] Radim Nencka,*[,†] and Evzen Boura*[,†]

[†]Institute of Organic Chemistry and Biochemistry, Academy of Sciences of the Czech Republic, v.v.i, Flemingovo nám. 2, 166 10 Prague 6, Czech Republic

[‡]Department of Chemistry of Natural Compounds, Institute of Chemical Technology Prague, Technicka 5, Prague 166 28, Czech Republic

Supporting Information

ABSTRACT: The lipid kinase phosphatidylinositol 4-kinase IIIβ (PI4KB) is an essential host factor for many positive-sense single-stranded RNA (+RNA) viruses including human pathogens hepatitis C virus (HCV), Severe acute respiratory syndrome (SARS), coxsackie viruses, and rhinoviruses. Inhibitors of PI4KB are considered to be potential broad-spectrum virostatics, and it is therefore critical to develop a biochemical understanding of the kinase. Here, we present highly potent and selective fluorescent inhibitors that we show to be useful chemical biology tools especially in determination of dissociation constants. Moreover, we show that the coumarin-labeled inhibitor can be used to image PI4KB in cells using fluorescence-lifetime imaging microscopy (FLIM) microscopy.

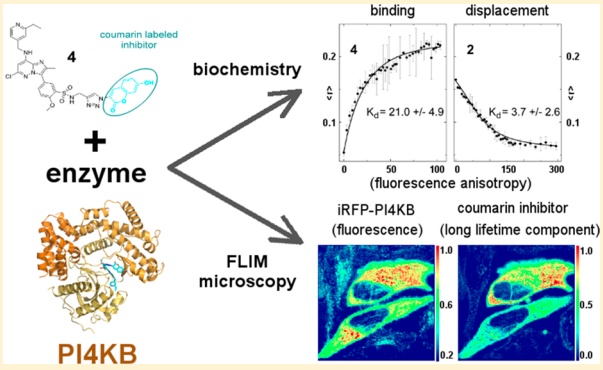

INTRODUCTION

Enzymes are among the most common targets for drugs (together with receptors and transporter proteins), and most drugs targeted to enzymes are inhibitors.[1] Therefore, thorough characterization of both the targeted enzymes and inhibitors is critical in developing their medicinal chemistry. Here, we focused on exploiting highly active and specific fluorescent inhibitors to characterize phosphatidylinositol 4-kinase IIIβ (PI4KB or PI4K IIIβ) and its inhibition both *in vitro* and *in vivo*.

PI4KB is one of four human enzymes responsible for the synthesis of phosphatidylinositol 4-phosphate (PI4P),[2−4] the most abundant phosphoinositide in human cells, a precursor for higher phosphoinositides, and a key signaling lipid itself.[5−7] PI4KB synthesizes the Golgi pool of PI4P and, together with PI4K2A, steers Golgi intracellular trafficking.[8,9] Notably, PI4KB was recently identified as an essential host factor for a plethora of positive-sense single-stranded RNA (+RNA) viruses.[10−15] These viruses include more or less dangerous human pathogens such as HCV, SARS, coxsackie viruses, and rhinoviruses, all of which hijack PI4KB to generate PI4P rich membranes that serve as their replication platforms (also known as replication organelles).[16] Because PI4Ks are implicated in human diseases, potent inhibitors were prepared by us and others,[17−19] and PI4Ks were also thoroughly structurally characterized[20−23] despite difficulties in crystallization of flexible proteins.[24] Here, we built upon our previously designed inhibitors as scaffolds (imidazopyridazine derivatives with methoxyphenylsulphoamide moiety) to design fluorescent inhibitors against PI4KB via attachment of a fluorescein or coumarin moiety.

For obvious health and safety reasons, fluorescence-based assays are increasingly replacing radioactivity-based assays in laboratory labeling. And indeed, we exclusively utilize luminescent ADP-Glo kinase assays[25] to characterize the functional enzymatic properties of our kinases of interest. However, in these assays the measured IC_{50} values are very dependent on the exact conditions in the reaction (e.g., ATP and substrate concentration). Therefore, often different laboratories report numbers that are difficult to compare because of differences in biochemical assays used. The apparent dissociation constant (K_D) would be a more useful value to report for every inhibitor that is being characterized. Although, K_D is inherently more difficult to measure than IC_{50}, fluorescent inhibitors are powerful tools to obtain the dissociation constants of enzyme−inhibitor complexes.[26] The synthesis of such fluorescent inhibitors is of widespread interest but often is limited to only basic microscopy assays.[27−30] Here, we apply our developed specific and potent fluorescent inhibitors to more complex tasks including biochemical enzyme characterization and fluorescence-lifetime imaging microscopy (FLIM).

RESULTS AND DISCUSION

Design of Fluorescent Inhibitors. We harnessed the general inhibitor scaffold from our previous and cosubmitted studies[17,41] and applied it to the design of fluorescent inhibitors. First, we prepared an alkyne derivative, **1**, which displays

Received: October 10, 2016
Published: December 8, 2016

DOI: 10.1021/acs.jmedchem.6b01466
J. Med. Chem. 2017, 60, 119−127

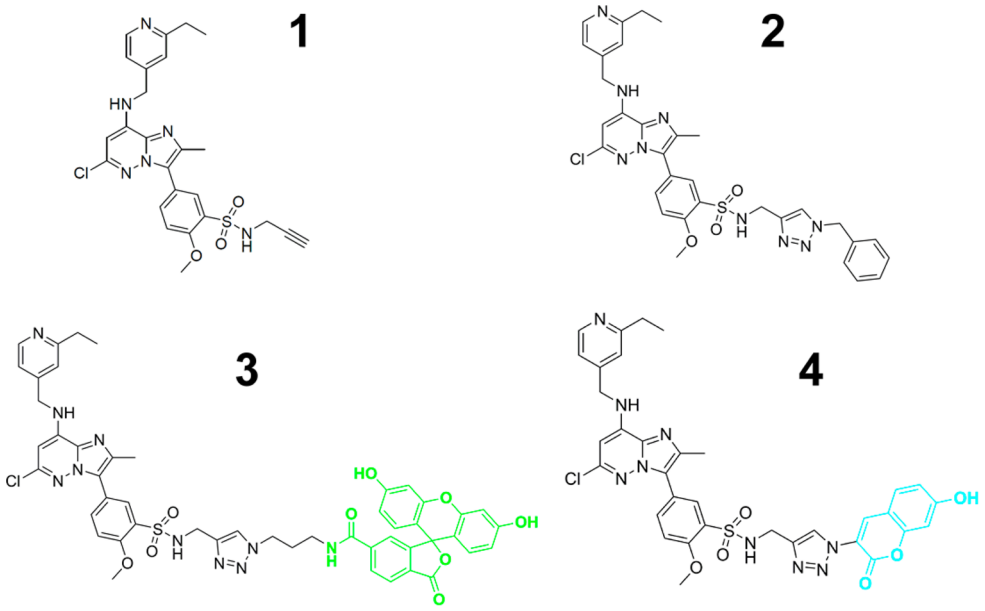

Figure 1. Prepared compounds. Fluorescein side chain is highlighted in green; coumarin side chain is highlighted in blue.

Scheme 1. Preparation of Compounds 1−4[a]

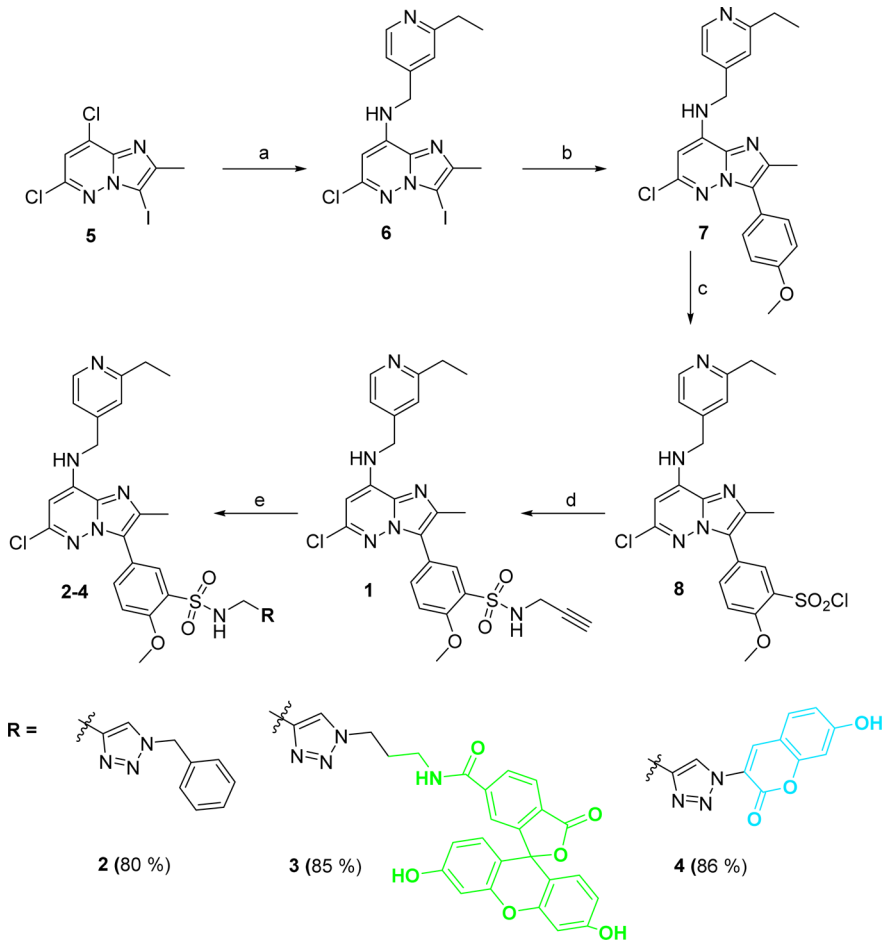

[a]Reagents and conditions: (a) (2-ethylpyridin-4-yl)methanamine, DIPEA, EtOH, 75 °C, ON; (b) (4-methoxyphenylboronic acid, $Pd(dppf)Cl_2$, Na_2CO_3,dioxane/H_2O 4:1, 95 °C, ON; (c) HSO_3Cl, DCM, 0 °C to rt, 4 h; (d) propargylamine, DCM, TEA, 0 °C to rt, 1 h; (e) azide, $CuSO_4 \cdot 5H_2O$, Na-ascorbate, THF/H_2O 1:1, rt, 2 h.

excellent properties *in vitro* (PI4KB IC_{50} = 13.4 ± 1.1 nM) and selectivity (PI4KA residual activity = 102% ± 6%) and subjected it to Cu(II)-catalyzed (Huisgen−Meldal) click reaction conditions with common fluorescent azide-tagged

DOI: 10.1021/acs.jmedchem.6b01466
J. Med. Chem. 2017, 60, 119−127

fluorescein and coumarin moieties. We sought to label the inhibitor in this manner with fluorophores easily excited by standard confocal microscopes. The fluorescein excitation peak is around the 488 nm laser line, and that of coumarin the 405 nm laser line, two lasers common in confocal microscopes. We employed a similar click procedure as in Mejdrova et al.[41] to generate compounds **2** (nonfluorescent inhibitor with small aromatic substituent), **3** (fluorescein labeled inhibitor), and **4** (coumarin labeled inhibitor) (Figure 1). The synthesis is described in Scheme 1. All three compounds retained excellent IC_{50} values (208.5 ± 14.7 nM for **2**, 39.4 ± 16.9 nM for **3**, and 76.3 ± 6.8 nM for **4**) of PI4KB.

Chemistry. 6,8-Dichloro-3-iodo-2-methylimidazo[1,2-*b*]-pyridazine **5** (prepared as described previously[31]) was substituted selectively at position 8 with (2-ethylpyridin-4-yl)methanamine (DIPEA, EtOH, 70 °C) affording derivative **6**. *p*-Methoxyphenyl derivative **7** prepared via Suzuki coupling was chlorosulfonated (HSO_3Cl, DCM, 0 °C) in the next step, and the crude sulfonyl chloride **8** was substituted with propargylamine (DIPEA, DCM) to afford propargyl sulfonamide **1**. Compound **1** was then reacted with the corresponding azide under Huisgen–Meldal click reaction conditions ($CuSO_4 \cdot 5H_2O$, sodium ascorbate, THF/H_2O, rt) providing triazoles **2**–**4**.

Membrane Permeability of Prepared Fluorescent Inhibitors. Compounds that exhibit robust membrane permeability are more useful for cell culture experiments because they easily penetrate into the cell's interior. Therefore, we tested the membrane permeability of our fluorescent compounds. We used the giant unilamellar vesicles (GUVs) biomimetic system that is ideal for imaging using confocal microscopy with only a small amount of fluorescent lipid (ATTO647N-DOPE at 0.1 mol % concentration). To determine the degree of membrane penetration of the fluorescein and coumarin labeled inhibitors **3** and **4**, the GUVs were imaged under a confocal microscope (Figure 2). Only coumarin labeled inhibitor **4**, exhibited good membrane permeability. It is important to note that it did not actually show particular preference for the lipid bilayer; however it did quickly diffuse through. Fluorescein tagged compound **3** was not able to cross the lipid bilayer. One of the two hydroxyl groups becomes charged (pK_a = 6.4) under physiological pH used in the experiment. Despite the overall hydrophobicity of compound **3**, these charged hydroxyl groups are detrimental for membrane permeability, preventing its use in standard intracellular imaging. Therefore, for the remaining studies, we employed only coumarin containing compound **4** due to its excellent properties in both fluorescence and permeability.

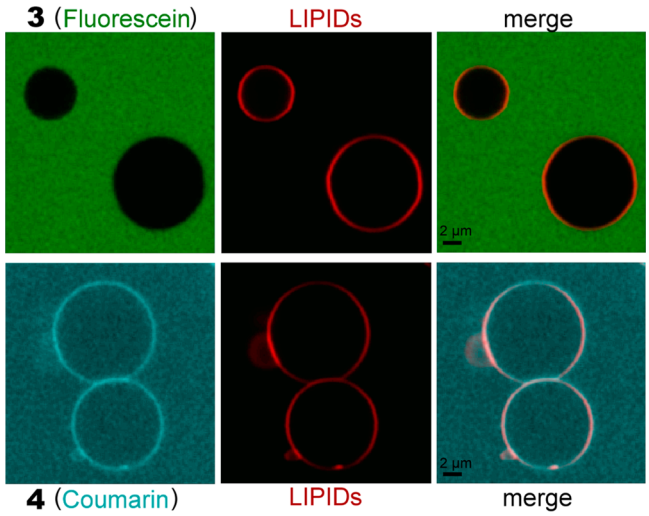

Figure 2. Membrane permeability of compounds **3** and **4**. Upper panels, fluorescence of compound **3** in green; lower panels, fluorescence of compound **4** in blue. ATTO647N-DOPE containing GUVs in red; scale bar 2 μm.

Determination of Dissociation Constants (K_D) of Fluorescent and Nonfluorescent Inhibitors. Changes in fluorescence properties can be used to determine the K_D of a fluorescent ligand with a macromolecule such as a protein. Most commonly, these are changes in the fluorescence intensity or anisotropy (or polarization) or the mean lifetime of the excited state (further on referred to as lifetime). Fluorescence anisotropy is usually the method of choice when studying binding of a small fluorescent molecule to a nonlabeled macromolecule because it is universal, robust, concentration independent, and easily accessible on most commercial fluorimeters.[32,33]

When randomly oriented, fluorescent molecules interact with polarized light; only those that have an excitation dipole moment parallel with polarization of light are excited resulting in an anisotropic situation that also manifests itself in emission (light is not emitted equally in all directions). Rotational motion of a fluorophore rearranges the dipoles back to the random orientation. Small, fast rotating fluorescence ligands therefore exhibit negligible anisotropy of fluorescence. However, a large molecule such as a fluorescent protein or a protein-bound fluorophore rotates slowly and does not reorient within the fluorescence lifetime and thus exhibits high anisotropy. Here, we titrated compound **4** with PI4KB while monitoring the increasing anisotropy of fluorescence to determine the K_D. The result was K_D of 21.0 ± 4.9 nM (Figure 3A), which is actually in good agreement with the IC_{50} value (76.3 ± 6.8 nM) from our biochemical assay. However, IC_{50} value depends strongly on the assays used, while K_D is a thermodynamic constant.

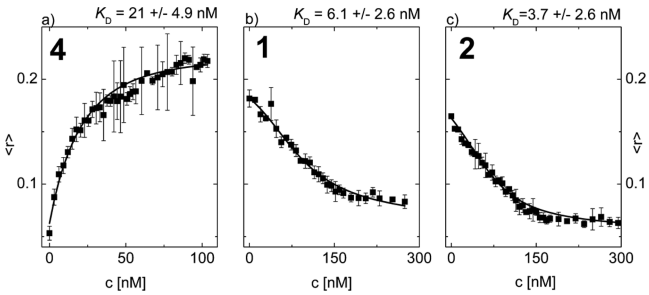

Figure 3. Determination of dissociation constants. (A) Compound **4** was titrated with PI4KB, and the anisotropy of fluorescence was measured. (B) Compound **4** was mixed with PI4KB, the nonfluorescent inhibitor **1** was titrated in, and the anisotropy of fluorescence was measured. (C) As in panel B except the nonfluorescent inhibitor **2** was used.

Again, when a fluorescent inhibitor is bound to its protein ligand, the resulting anisotropy of fluorescence is high because it cannot rotate freely. However, when a nonfluorescent competitor is titrated in the reaction the anisotropy decreases as the fluorescent inhibitor is liberated from the protein by a nonfluorescent competitor. We used this principle to measure

DOI: 10.1021/acs.jmedchem.6b01466
J. Med. Chem. 2017, 60, 119–127

the K_D of nonfluorescent inhibitors (compounds **1** and **2**). The resulting K_D values were 6.1 ± 2.6 and 3.7 ± 2.6 nM (Figure 3B,C), which is in good agreement with the IC_{50} value for **1** (13.6 ± 0.7 nM) but not so much for compound **2** IC_{50} value (208.5 ± 14.7 nM). Importantly, such titrations could be performed robotically or in 384 well plate format, and a script could be written to allow automatic data processing suggesting that the above-described assay can be used in high-throughput screening. In other words, one fluorescent inhibitor is enough to determine the K_D of any other nonfluorescent competitive inhibitors.

Spectral Properties Deem Compound 4 as Ideal for FLIM. Coumarin-based derivatives are well-established microenvironment sensing probes.[34] Their excited state energy is decreased over the course of time (femtosecond to nanosecond) due to the rearrangement of solvent dipoles. This results in high sensitivity of its emission spectra to the polarity and mobility of solvent molecules in close vicinity to the probe. Consequently, lifetime and quantum yield of coumarins at a given emission wavelength also reflect the local dye environment.[35] While the change of the quantum yield was a small obstacle during the anisotropy measurements (one parameter must be added to account for different quantum yields of the bound and unbound states as detailed in the Experimental Methods section), the change in the lifetime is very advantageous for microscopy as it enables us to distinguish subpopulations of the fluorophore based on different lifetime values.

A docking experiment using compound **4** revealed that the coumarin moiety is localized in close vicinity to the surface of the PI4KB kinase (Figure 4A) suggesting that the microenvironment of a protein-bound fluorophore will be different and a change in fluorescence properties is to be expected. Indeed, the emission spectra of compound **4** are red-shifted (emission peak 422 versus 470 nM) in the presence of PI4KB (Figure 4B). Next, we investigated the changes in lifetime. We observed that the lifetime of compound **4** increases when PI4KB is titrated into the cuvette, from 0.96 ns when compound **4** is in the buffer to 2.46 ns when fluorescent inhibitor **4** is fully saturated by the PI4KB enzyme (Figure 4C). This change is specific as the addition of noninteracting protein BSA does not affect the lifetime (Figure 4D).

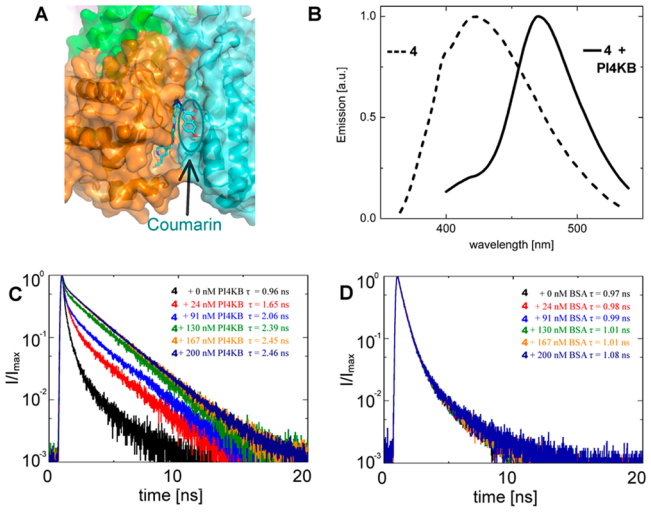

Figure 4. Spectral properties of compound **4**. (A) Compound **4** docked in the active site of PI4KB; coumarin side chain is highlighted. (B) Fluorescence emission spectra of compound **4**. (C) Lifetime of compound **4** in the presence of increasing amount of PI4KB. (D) Lifetime of compound **4** in the presence of increasing amount of BSA.

FLIM Microscopy. Because of the suitable fluorescence properties of compound **4** for FLIM *in vitro*, we tested it in cells. We sought to determine if compound **4** would be able to specifically recognize PI4KB in living cells. For this reason, we prepared a plasmid that encoded PI4KB fused to the fluorescent protein iRFP (iRFP-PI4KB). We transfected the HeLa cells with the iRFP-PI4KB plasmid and 24 h later incubated them with compound **4** for 30 min. Then the medium was exchanged for PBS, and the fluorescence of iRFP and compound **4** was observed (Figure 5A,B, SI Figure 1). The results suggested that compound **4** is not only bound to iRFP-PI4KB but also present in high amounts elsewhere, especially in vesicles (Figure 5B). However, when the same experiment was done in the FLIM mode, we observed the coumarin signal with the highest lifetime value (2 ns, corresponding to compound **4** bound to PI4KB *in vitro*) only at the spots where we also observed the highest iRFP fluorescence (Figure 5A,C). Moreover, the spatial distribution resembled the Golgi where PI4KB is normally localized. When only the long lifetime of the coumarin labeled inhibitor (corresponding lifetime of PI4KB bound compound **4**) is filtered (Figure 5D), then the signal distribution is essentially the same as the fluorescence signal of iRFP-PI4KB. These data suggest that compound **4** can be used to observe PI4KB in a FLIM experiment.

CONCLUSIONS

We show that our imidazopyridazine scaffolds derivatized with *ortho*-methoxyphenylsulfoamide moiety are suitable to prepare highly potent and selective fluorescent inhibitors via rather simple click chemistry. Such compounds are powerful tools to characterize enzymes and nonfluorescent inhibitors *in vitro*. Additionally, we show that they are also powerful tools in FLIM microscopy when an environmentally sensitive fluorophore such as coumarin is used to label the inhibitor. In principle, our approach can be used for any enzyme given that a suitable potent and selective inhibitor is available.

EXPERIMENTAL METHODS

Synthesis of Novel Inhibitors. *General Chemical Procedures.* NMR spectra were measured on Bruker Avance II-600 or Bruker Avance II-500 instruments (600.1 or 500.0 MHz for ^{1}H and 150.9 or 125.7 MHz for ^{13}C) in hexadeuterodimethyl sulfoxide and referenced to the solvent signal (□ 2.50 and 39.70, respectively). Mass spectra were measured on a LTQ Orbitrap XL (Thermo Fischer Scientific) using electrospray ionization (ESI) and a GCT Premier (Waters) using EI. The elemental analyses were obtained on a PerkinElmer CHN Analyzer 2400, Series II Sys (PerkinElmer) and X-ray fluorescence spectrometer SPECTRO iQ II (SPECTRO Analytical Instruments, Germany). Column chromatography and thin-layer chromatography (TLC) were performed using silica gel 60 (Fluka) and Silufol silica gel 60 F_{254} foils (Merck), respectively. Solvents were evaporated at 2 kPa and bath temperature 30−60 °C. The compounds were dried at 13 Pa and 50 °C. The purity of the compounds was determined either by elemental analysis or by HPLC and all compounds exhibited ≥95% purity.

General Procedure: Click Reaction. Alkyne derivative **1** was dissolved in THF/H_2O (1:1 v/v), and azide (1 equiv) was added. The reaction mixture was degassed at 0 °C and flushed with argon, and $CuSO_4 \cdot 5H_2O$ (5 mol %) and sodium ascorbate (10 mol %) were added in one portion. Additional ligand was added if necessary as specified below. The reaction mixture was stirred at room temperature

DOI: 10.1021/acs.jmedchem.6b01466
J. Med. Chem. 2017, 60, 119−127

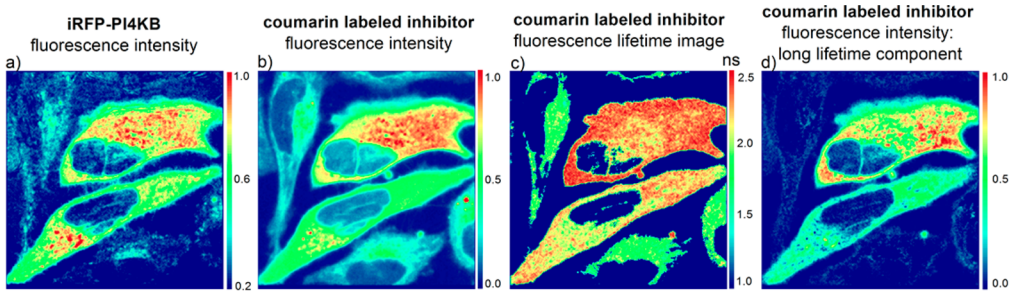

Figure 5. Colocalization of fluorescent inhibitor **4** with transiently expressed iRFP-PI4KB in living HeLa cells. (A) Fluorescence intensity of iRFP-PI4KB. (B) Fluorescence intensity of compound **4**. (C) Fluorescence lifetime distribution of compound **4**. (D) Intensity fraction corresponding to the lifetime of the protein bound coumarin labeled inhibitor.

and monitored by TLC. After completion of the reaction, the mixture was diluted with EtOAc (20 mL/015 mmol of **1**) and washed with water. The aqueous phase was extracted twice more with EtOAc (2 × 10 mL), and the combined organic phases were dried over Na_2SO_4 and evaporated under reduced pressure. The residue was purified by flash column chromatography (SiO2, EtOAc/EtOH).

*5-(6-Chloro-8-(((2-ethylpyridin-4-yl)methyl)amino)-2-methylimidazo[1,2-b]pyridazin-3-yl)-2-methoxy-N-(prop-2-yn-1-yl)-benzenesulfonamide (**1**).* Derivative **8** (0.3 g, 0.592 mmol) was dissolved in dry DCM (15 mL), and DIPEA (155 μL, 1.5 equiv) was added followed by an addition of prop-2-yn-1-amine (57 μL, 1.5 equiv). Reaction mixture was stirred overnight at rt, adsorbed onto silica gel, and purified by column chromatography. Mobile phase: EtOAc/EtOH (20−50%). Yield: 107 mg (78%); mp 216.1−217.5 °C. ^{1}H NMR (400 MHz, DMSO-d_6) δ (ppm): 8.54 (t, J_{NH-CH2} = 6.4 Hz, 1 H, NH-8″), 8.41 (dd, $J_{6‴-5″}$ = 5.1 Hz,$J_{6‴-3‴}$ = 0.6 Hz, 1 H, H-6‴), 7.97 (d, J_{6-4} = 2.3 Hz, 1 H, H-6), 7.87 (dd, J_{4-3} = 8.7 Hz, J_{4-6} = 2.3 Hz, 1 H, H-4), 7.37 (d, J_{3-4}= 8.7 Hz, 1 H, H-3), 7.25 (bs, 1 H, H-3‴), 7.17 (dd, $J_{5‴-6‴}$ = 5.1 Hz, $J_{5‴-3‴}$ = 1.4 Hz, 1 H, H-5‴), 6.15 (s, 1 H, H-7″), 4.60 (bs, 2 H, 8″-NH-C**H**$_2$), 3.97 (s, 3 H, 2-OCH$_3$), 3.77 (dd, $J_{1′-NH}$ = 6.0 Hz, $J_{1′-3′}$ = 2.4 Hz, 2 H, H-1′), 2.98 (t, $J_{3′-1′}$ = 2.4 Hz, 1 H, H-3′), 2.72 (q, $J_{CH2-CH3}$ = 7.6 Hz, 2 H, C**H**$_2$-CH$_3$), 2.44 (s, 3 H, 2″-CH$_3$), 1.20 (t, $J_{CH2-CH3}$ = 7.6 Hz, 3 H, CH$_2$C**H**$_3$). ^{13}C NMR (125 MHz, DMSO-d_6) δ (ppm): 162.94 (C-2‴), 156.15 (C-2), 149.14 (C-6″), 147.85 (C-4‴), 147.02 (C-6″), 143.08 (C-8″), 137.98 (C-2″), 135.14 (C-4), 131.08 (C-9″), 129.80 (C-6), 128.50 (C-1), 123.75 (C-3″), 120.43 (C-3‴), 120.32 (C-5), 119.59 (C-5‴), 113.24 (C-3), 91.83 (C-7″), 79.87 (C-2′), 74.1 (C-3′), 56.54 (2-O−CH$_3$), 44.32 (8″-NH-**C**H$_2$), 32.28 (C-1′), 30.67 (**C**H$_2$−CH$_3$), 14.50 (2′-CH$_3$), 13.89 (CH$_2$−**C**H$_3$). Anal. (C$_{25}$H$_{25}$ClN$_6$O$_3$S.0.33EtOAc) C, H, N. HRMS: calcd for [M + H], 525.14701; found, 525.14705. 1/3 EtOAc: C, 57.05; H, 5.03; N, 15.16. Found: C, 56.99; H, 4.81; N, 15.49.

*N-((1-Benzyl-1H-1,2,3-triazol-4-yl)methyl)-5-(6-chloro-8-(((2-ethylpyridin-4-yl)methyl)amino)-2-methylimidazo[1,2-b]pyridazin-3-yl)-2-methoxybenzenesulfonamide (**2**).* Mobile phase: EtOAc/EtOH (0−20%). Yield: 60 mg (80%) as an off-white foam. ^{1}H NMR (500 MHz, DMSO-d_6) δ (ppm): 8.58 (t, J_{NH-CH2} = 6.2 Hz, 1 H, 8′-NH), 8.41 (bs, 1 H, H-6″), 7.93 (d, J_{6-4} = 2.3 Hz, 1 H, H-6), 7.86 (t, J_{NH-CH2} = 6.2 Hz, 1 H, SO$_2$NH), 7.79 (dd, J_{4-6} = 2.3 Hz, J_{4-5} = 8.6 Hz, 1 H, H-4), 7.68 (s, 1 H, H-5‴), 7.23−7.31 (m, 4 H, H-3″, H-3‴, H-4‴), 7.15−7.21 (m, 4 H, H-3, H-5″, H-2‴), 6.14 (s, 1 H, H-7′), 5.42 (s, 2 H, NH−CH $_2$), 4.60 (bs, 2 H, NH−CH$_2$−4″), 4.16 (d, J_{CH2-NH} = 6.2 Hz, 2 H, SO$_2$NH−CH$_2$), 3.82 (s, 3 H, 2-O−CH$_3$), 2.72 (q, $J_{CH2-CH3}$ = 7.6 Hz, 2 H, C**H**$_2$-CH$_3$), 2.44 (s, 3 H, 2′-CH$_3$), 1.20 (t, $J_{CH2-CH3}$ = 7.6 Hz, 3 H, CH$_2$−C**H**$_3$). ^{13}C NMR (125 MHz, DMSO-d_6) δ (ppm): 163.02 (C-2″), 155.73 (C-2), 149.25 (C-6″), 147.75 (C-4″), 147.03 (C-6′), 143.99 (C-4‴), 143.12 (C-8′), 137.96 (C-2′), 135.89 (C-1‴), 134.99 (C- 4), 131.07 (C-9′), 129.87 (C-6), 128.80 (C-3‴), 128.44 (C-1), 128.23 (C-2‴, 4‴), 123.79 (C-3′), 123.23 (C-5‴), 120.42 (C-3″), 120.20 (C-5″), 119.60 (C-5″), 112.99 (C-3), 91.83 (C-7′), 56.37 (2-O−CH$_3$), 52.81 (N−CH$_2$), 44.31 (NH−CH$_2$−4″), 38.29 (SO$_2$NH−CH$_2$), 30.76 (**C**H$_2$CH$_3$), 14.48 (2′-CH$_3$), 13.93 (CH$_2$−**C**H$_3$). Anal. (C$_{32}$H$_{32}$ClN$_9$O$_3$S.EtOH) C, H, N. HRMS: calcd for [M + H], 658.21101; found, 658.21053. EtOH: 57.99; H, 5.44; N, 17.90. Found: C, 57.66; H, 5.17; N, 17.77.

*N-(3-Azidopropyl)-3′,6′-dihydroxy-3-oxo-3H-spiro-[isobenzofuran-1,9′-xanthene]-6-carboxamide (**3**).* Derivative **3** was prepared according to general procedure 1. Additional ligand BTTP, 10 mol %, was added. Subsequently, it was purified by reverse phase flash column chromatography using C18-silica gel, mobile phase CH$_3$CN/H$_2$O (50−100%). Yield 10 mg (80%) as a yellow solid. ^{1}H NMR (400 MHz, DMSO-d_6) δ (ppm): 10.15 (s, 1 H, OH), 8.70 (t, J = 5.5 Hz, 1 H, NHCO), 8.55 (t, J = 6.7 Hz, 1 H, 8‴″′-NH), 8.41 (s, 1 H, SO$_2$NH), 8.18−8.04 (m, 1 H, H4), 7.91 (d, J = 2.3 Hz, 1 H, H-6‴), 7.83 (d, J = 6.2 Hz, 1 H, H-4‴), 7.76 (dd, J = 8.6, 2.3 Hz, 1 H), 7.70 (s, 1 H, H-5), 7.66 (s, 1 H), 7.27−7.20 (m, 2 H), 7.16 (d, J = 5.0 Hz, 1 H, H-7), 6.69 + 6.59 (d+m, 6 H, H-8′, 7′, 1′, 2, 4′, 5′), 6.13 (s, 1 H, H-3‴″), 4.57 (br s, 1 H, CH$_2$NH), 4.21 (t, J = 7.0 Hz, 2 H), 4.14 (d, J = 5.4 Hz, 2 H), 3.87 (s, 3 H), 3.15 (q, J = 6.6 Hz, 2 H), 2.75−2.68 (m, 2 H), 2.41 (s, 3H), 2.11 (s, 1 H), 1.91 (p, J = 7.0 Hz, 2 H), 1.19 (t, J = 7.5 Hz, 3 H), 1.14 (s, 2 H). ^{13}C NMR (125 MHz, DMSO-d_6) δ (ppm): 168.51 (C-3), 165.13 (C-6), 163.31 (C-2‴″), 160.17 (C-3′), 156.06 (C-2‴), 153.02 (C-2), 152.32 (C-4′a, C-5′a), 147.99 (C-4‴″), 147.30 (C-6‴′), 143.82 (C-8‴′), 143.39 (C-4‴), 141.01, 138.23 (C-2‴′), 135.23, 131.34 (C-9‴′), 130.12, 129.82, 129.73, 128.80, 125.35, 124.04 (C-3‴′), 123.60 (C-5‴), 122.74. 120.51 (C-1‴), 113.26, 109.63 (C1′a, C8′a), 102.72, 63.26, 56.72 (OCH$_3$), 56.30, 47.56 (C-3″), 44.59, 38.59 (NH−CH$_2$), 37.23 (C-1″), 31.04 (CH$_2$CH$_3$), 30.07, 30.02 (C-2″), 14.72 (2‴′CH$_3$), 14.21(CH$_2$CH$_3$). HRMS: calcd for [M + H], 983.26965; found, 983.27003.

*5-(6-Chloro-8-(((2-ethylpyridin-4-yl)methyl)amino)-2-methylimidazo[1,2-b]pyridazin-3-yl)-N-((1-(7-hydroxy-2-oxo-2H-chromen-3-yl)-1H-1,2,3-triazol-4-yl)methyl)-2-methoxybenzenesulfonamide (**4**).* Compound **1** (26 mg, 0.0495 mmol) was combined with 3-azido-7-hydroxy-2*H*-chromen-2-one (10 mg, 1 equiv), and the mixture of *t*-BuOH/H$_2$O (0.8 mL, 1:1) was added. The suspension was degassed and CuSO$_4$·5H$_2$O (0.6 mg, 5 mol %) together with BTTP (10 mol %) was added quickly. After a few minutes Na-ascorbate (1 mg, 10 mol %) was added, and the mixture was stirred at rt for 1 h. The completion of the reaction was monitored by TLC (EtOAc). The mixture was further diluted with water and extracted with EtOAc. Organic phases were dried over sodium sulfate, and the residue was purified by flash column chromatography (mobile phase EtOAc/EtOH 0−10%). Yield 30 mg (86%) as an off-white solid; mp 236.0−238.2 °C. ^{1}H NMR (500 MHz, DMSO-d_6) δ (ppm): 8.50 (t, J_{NH-CH2} = 6.3 Hz, 1 H, 8‴-NH), 8.41 (dd, $J_{6‴-5‴}$ = 5.2 Hz, 1 H, H-6‴), 8.37 (s, 1 H, H-4″), 8.25 (s, 1 H, H-5′), 7.97 (t, J_{NH-CH2} = 6.1 Hz, 1 H, SO$_2$−NH), 7.93 (d, J_{6-4} = 2.3 Hz, 1 H, H-6), 7.80 (dd, J_{4-6} = 2.3 Hz, J_{4-3} = 8.7 Hz, 1 H, H-4), 7.67 (d, $J_{5″-6″}$ = 8.7 Hz, 1 H, H-5″), 7.27 (d, J_{3-4} = 8.7 Hz, 1 H, H-3), 7.25 (bs, 1 H, H-3‴), 7.15 (dm, $J_{5‴-6‴}$ = 5.2 Hz, 1 H, H-5‴), 6.88 (dd, $J_{6″-5″}$ = 8.7 Hz, $J_{6″-8″}$ = 2.2 Hz, 1 H, H-6″), 6.79 (d, $J_{8″-6″}$ = 2.2 Hz, 1 H, H-8″), 6.08 (s, 1 H, H-7‴), 4.58 (bs, 2 H, 8‴-NH−CH$_2$), 3.94 (s, 3 H, O−CH$_3$), 2.72 (q, $J_{CH2-CH3}$ = 7.6 Hz, 2 H, CH$_2$−CH$_3$), 2.41 (s, 3 H, 2‴-CH$_3$), 1.20 (t, $J_{CH2-CH3}$ = 7.6 Hz, 3 H, CH$_2$−C**H**$_3$). ^{13}C NMR (125 MHz, DMSO-d_6) δ (ppm): 162.96 (C-2‴), 162.57 (C-7″), 156.13 (C-2″), 155.68 (C-2), 154.62 (C-8″a), 149.18 (C-6‴), 147.86 (C-4‴), 146.95 (C-6‴), 143.84 (C-

DOI: 10.1021/acs.jmedchem.6b01466
J. Med. Chem. 2017, 60, 119−127

4′), 143.02 (C-8‴), 137.93 (C-2‴), 135.78 (C-4″), 134.74 (C-4), 131.00 (C-9‴), 130.98 (C-5″), 129.47 (C-6), 128.51 (C-1), 124.22 (C-5′), 123.57 (C-3‴), 120.43 (C-3⁗), 120.22 (C-5), 119.57 (C-5⁗), 119.12 (C-6″), 114.41 (C-6″), 113.04 (C-3), 110.37 (C-4″a), 102.25 (C-8″), 91.74 (C-7‴), 56.50 (O−CH_3), 44.33 (8‴CH_2NH), 30.70 (CH_2−CH_3), 14.59 (2‴-CH_3), 13.94 (CH_2−CH_3). Anal. ($C_{34}H_{30}ClN_9O_6S.H_2O$) C, H, N. HRMS: calcd for [M + H], 728.18010; found, 728.18039. H_2O: C, 54.73; H, 4.32; N, 16.89. Found: C, 54.60; H, 4.68; N, 16.29.

*6,8-Dichloro-3-iodo-2-methylimidazo[1,2-b]pyridazine (**5**).* Title compound was prepared according to described procedure.[31]

*6-Chloro-N-((2-ethylpyridin-4-yl)methyl)-3-iodo-2-methylimidazo[1,2-b]pyridazin-8-amine (**6**).* Derivative **5** (150 mg, 0.47 mmol) was dissolved in ethanol (5 mL) and DIPEA (0.25 mL, 1.41 mmol, 3 equiv) together with (2-ethylpyridin-4-yl)methanamine (128 mg, 2 equiv). The reaction mixture was then stirred at 75 °C for 12 h (or until consumption of the starting material as indicated by TLC, mobile phase petroleum ether/EtOAc 1:1). The reaction mixture was then concentrated and adsorbed directly onto silica gel and purified. Mobile phase petroleum ether/EtOAc (60−90%). Yield: 1.205 g (85%) as yellowish solid; mp 144.2−145.3 °C. ^{1}H NMR (400 MHz, DMSO-d_6) δ (ppm): 8.54 (t, J_{NH-CH2} = 6.1 Hz, 1 H, NH), 8.39 (d, $J_{6'-5'}$ = 5.0 Hz, 1 H, H-6′), 7.21 (s, 1 H, H-3′), 7.13 (d, $J_{5'-6'}$ = 5.0 Hz, 1 H, H-5′), 6.16 (s, 1 H, H-7), 4.57 (bs, 2 H, C**H**$_2$-NH), 2.70 (q, $J_{CH2-CH3}$ = 7.4 Hz, 2 H, CH_2CH_3), 2.37 (s, 3 H, 2-CH_3), 1.18 (t, $J_{CH3-CH2}$ = 7.4 Hz, 3 H, CH_2CH_3). ^{13}C NMR (125 MHz, DMSO-d_6) δ (ppm): 162.99 (C-2′), 149.19 (C-6′), 147.71 (C-6), 144.01 (C-2), 142.92 (C-8), 134.22 (C-9), 120.42 (C-3′), 119.60 (C-5′), 92.32 (C-7), 72.02 (C-3), 44.35 (NH-**C**H_2), 30.70 (**C**H_2−CH_3), 14.90 (2-CH_3), 13.95 (CH_2−**C**H_3). Anal. ($C_{15}H_{15}ClIN_5$) C, H, N. HRMS: calcd for [M + H], 506.08149; found, 506.08148.

*6-Chloro-N-((2-ethylpyridin-4-yl)methyl)-3-(4-methoxyphenyl)-2-methylimidazo[1,2-b]pyridazin-8-amine (**7**).* Iodo derivative **6** (313 mg, 0.732 mmol) was suspended in 1,4-dioxane (8 mL) followed by an addition of (4-methoxyphenyl)boronic acid (122 mg, 1.1 equiv), and solution of 1 M Na_2CO_3 (2 mL) was added. Reaction mixture was degassed three times, Pd(dppf)Cl_2 (15 mg, 5 mol %) was added quickly, and the mixture was degassed once more, heated up to 90 °C, and stirred until the completion of the reaction (overnight). After cooling to rt, the mixture was diluted with water/brine 1:1 and extracted with DCM, and the water phase was extracted twice more. Combined organic phases were dried over sodium sulfate, evaporated, and purified by flash column chromatography providing compounds **7**. Mobile phase (EtOAc/EtOH 0−10%). Yield: 0.987 g (90%) as an off-white solid; mp 168.8−169.1 °C. ^{1}H NMR (400 MHz, DMSO-d_6) δ (ppm): 8.51 (t, J_{NH-CH2} = 6.2 Hz, 1 H, NH), 8.40 (d, $J_{6''-5''}$ = 5.1 Hz, 1 H, H-6″), 7.55 (m, 2 H, H-2′), 7.24 (bs, 1 H, H-3″), 7.16 (dd, $J_{5''-6''}$ = 5.1 Hz, $J_{5''-3''}$ = 1.4 Hz,1H, H-5″), 7.08 (m, 2 H, H-3′), 6.10 (s, 1H, H-7), 4.58 (bs, 2 H, C**H**$_2$-NH), 3.82 (s, 3 H, 4′-OCH_3); 2.71 (q, $J_{CH2-CH3}$ = 7.7 Hz, 2 H, C**H**$_2$$CH_3$), 2.42 (s, 3 H, 2-$CH_3$), 1.20 (t, 3 H, $J_{CH3-CH2}$ = 7.7 Hz, CH_2C**H**$_3$). ^{13}C NMR (125 MHz, DMSO-d_6) δ (ppm): 162.99 (C-2″), 159.04 (C-4′), 149.24 (C-6″), 147.84 (C-4″), 146.84 (C-6), 143.03 (C-8), 1387.48 (C-2), 130.75 (C-9), 130.71 (C-2′), 125.10 (C-3), 120.74 (C-1′), 120.41 (C-3″), 119.56 (C-5″), 114.14 (C-3′), 91.48 (C-7), 55.38 (4′-O−CH_3), 44.29 (NH-**C**H_2), 30.73 (**C**H_2−CH_3), 14.53 (2-CH_3), 13.93 (CH_2−**C**H_3). Anal. ($C_{22}H_{22}ClN_5O.0.5EtOH$) C, H, N. HRMS: calcd for [M + H], 408.15856; found, 408.15868.

*5-(6-Chloro-8-(((2-ethylpyridin-4-yl)methyl)amino)-2-methylimidazo[1,2-b]pyridazin-3-yl)-2-methoxybenzenesulfonyl chloride (**8**).* Compound 7 (270 mg, 0.662 mmol) was dissolved in dry DCM (5 mL) cooled in an ice/brine mixture, and chlorosulfonic acid (4 mL, in excess) was added slowly. Reaction mixture was stirred in ice bath for another 30 min and then allowed to warm to rt after which it was stirred another 4 h. The reaction mixture was poured carefully onto ice, pH was adjusted to 7 with saturated $NaHCO_3$ solution, and the mixture was extracted with DCM, 3×. Combined organic phases were dried over sodium sulfate and evaporated, and the crude product was used without further purification since no starting material was detected (TLC, satisfied purity of ^{1}H NMR). Analytical sample was obtained after the flash column chromatography.

Mobile phase: EtOAc/EtOH (10−15%) as an off-white solid; mp 258 °C (decomp). ^{1}H NMR (400 MHz, DMSO-d_6) δ (ppm): 8.47 (dm, $J_{6''-5''}$ = 5.2 Hz, 1 H, H-6″), 8.14 (d, J_{6-4} = 2.3 Hz, 1 H, H-6), 8.01 (dd, J_{4-6} = 2.3 Hz,J_{4-3} = 8.7 Hz, 1 H, H-4), 7.21 (d, J_{3-4} = 8.7 Hz, H-3), 7.09 (bs, 1 H, H-3″), 7.04 (dm, $J_{5''-6''}$ = 5.2 Hz, 1 H, H-5″), 6.33 (m, 1 H, CH_2−N**H**), 5.89 (s, 1 H, H-7′), 4.49 (d, 2 H, J_{CH2-NH} = 6.1 Hz, 2 H, C**H**$_2$-NH), 4.06 (s, 3 H, OCH_3); 2.78 (q, $J_{CH2-CH3}$ = 7.6 Hz, 2 H, CH_2CH_3), 2.46 (s, 3 H, 2′-CH_3), 1.25 (t, $J_{CH3-CH2}$ = 7.6 Hz, 3 H, CH_2CH_3). ^{13}C NMR (125 MHz, DMSO-d_6) δ (ppm): 164.42 (C-2″), 156.69 (C-2), 149.75 (C-6″), 147.95 (C-6′), 145.69 (C-4″), 142.09 (C-8′), 138.95 (C-2′), 137.78 (C-4), 131.91 (C-5), 131.27 (C-9′), 130.33 (C-6), 123.63 (C-3′), 121.08 (C-1), 120.19 (C-3″), 119.17 (C-5″), 113.54 (C-3), 93.16 (C-7′), 56.85 (O−CH_3), 45.79 (NH-**C**H_3), 31.30 (**C**H_2−CH_3), 14.51 (2′-CH_3), 13.88 (CH_2−**C**H_3). Anal. ($C_{22}H_{21}Cl_2N_5O_3S$) C, H, N. HRMS: calcd for [M + H], 506.08149; found, 506.08148.

Biochemical and Biophysical Methods. *Protein Purification.* The PI4KB enzyme was prepared by bacterial expression as described previously[36] using standard protocols of our laboratory.[37,38] Briefly, *Escherichia coli* BL21 Star were transformed with 6xHisGB1 tagged PI4KB expression plasmid and grown at 37 °C to prepare inoculum. The next day, 12 L of autoinduction media was inoculated and grown at 37 °C until the OD reached 1; then temperature was lowered to 20 °C, and the bacteria were grown overnight. Subsequently, bacteria were lysed in lysis buffer (50 mM Tris, pH 8, 300 mM NaCl, 20 mM imidazole, 10% glycerol), and PI4KB was isolated by nickel affinity chromatography. The tag was removed by TEV protease, and PI4KB was further purified on Superdex 200 column (GE Healthcare) in SEC buffer (10 mM Tris, pH 8, 200 mM NaCl, 3 mM βME). PI4KB was concentrated to 5 mg/mL and stored in −80 °C until needed.

GUVs (Giant Unilamellar Vesicles). GUVs composed of POPC (99.9 mol %) (Avanti Polar lipids, Alabaster, AL) and ATTO647N-DOPE (0.1 mol %) (ATTO-TEC GmbH, Siegen, Germany) were prepared by electroformation as described previously.[39] Briefly, 50 μg of the lipid mixture was applied on each electrode (5 × 5 cm^2 ITO coated glass) and dried in vacuum overnight. The next day the coated glasses were moved to a homemade Teflon chamber, and 5 mL of 600 mM sucrose was added. Altering current with maximum voltage amplitude of 1 V, and frequency of 10 Hz was applied for 1 h. For imaging, 250 μL of GUVs and 250 μL of buffer (50 mM Tris, pH = 8, 300 mM NaCl, 1 mg/mL BSA) containing 100 nM compounds **3** or **4** were mixed.

Spectroscopy. The emission spectra and the steady state anisotropy of compound **4** were acquired on Fluoromax-4 fluorescence spectrometer (Horiba, Kyoto, Japan). For the anisotropy measurement, compound **4** was excited at 340 nm, and the emission was collected at 460 nm.

The measurements of the dissociation constants (K_D's) were carried out in citrate buffer (20 mM citrate buffer, 200 mM NaCl, 3 mM 2-mercaptoethanol). For the K_D(**4**) determination of fluorescent compound **4**, 50 nM solution of compound **4** in the citrate buffer was titrated with PI4KB so that the overall protein concentration varied from 3 to 100 nM. For the K_D(**2**) determination of nonfluorescent compound **2**, the mixture of 100 nM compound **4** and 100 nM PI4KB in citrate buffer was titrated by compound **2** so that its final concentration ranged from 0 to 250 nM.

The dependence of compound **4** fluorescence anisotropy on the concentration PI4KB was fitted by the formula

$$r = \frac{xqr_{bound} + (c_4 - x)r_{free}}{xq + (c_4 - x)} \quad (1)$$

where r_{bound} and r_{free} stand for anisotropy of compound **4** bound to PI4KB and free in solution, respectively, c_4 is the overall concentration of compound **4**, q is the ratio of fluorescence quantum yields of bound and free coumarin, and x is the concentration of bound compound **4** and results from solving of the chemical equilibrium:

DOI: 10.1021/acs.jmedchem.6b01466
J. Med. Chem. 2017, 60, 119−127

$$x = \frac{1}{2}(-(K_D(\mathbf{4}) + c_4 + c_{PI4KB}) - \sqrt{(K_D(\mathbf{4}) + c_4 + c_{PI4KB})^2 - 4c_4c_{PI4KB}}) \quad (2)$$

where c_{PI4KB} is the overall concentration of the PI4KB enzyme.

The replacement of fluorescent inhibitor **4** bound to PI4KB by a nonfluorescent inhibitor **2** leading to a decrease of anisotropy was also fitted by eq 1. Here x, the concentration of **4** bound to PI4KB, solves the equilibrium equations describing a system of a protein in the presence of two ligands with different binding affinity:

$$K_D(\mathbf{4}) = \frac{(c_{PI4KB} - x - y)(c_4 - x)}{x} \quad (3)$$

$$K_D(\mathbf{2}) = \frac{(c_{PI4KB} - x - y)(c_2 - y)}{y} \quad (4)$$

where y stands for the concentration of the nonfluorescent inhibitor **2** bound to PI4KB.

The fitting procedure as well as the analytical solution of eqs 3 and 4 were performed in Matlab (MathWorks, Natick, MA). The two dependencies were fitted globally sharing parameters $K_D(\mathbf{4})$, q, r_{bound}, and r_{free}.

Docking. The docking of the fluorescent inhibitor **4** was performed in similar fashion as previously described.[40] Briefly, the structure was prepared in ACD/ChemSketch 12.01 (Advanced Chemistry Development, Inc.), and the geometry was optimized with MOPAC2016 (Stewart Computational Chemistry, Colorado Springs, CO, USA, http://OpenMOPAC.net) using PM7 method. The necessary format conversions were performed using OpenBabel, and the docking was done using standard procedure in AutoDock Vina 1.1. We used the crystal structure with compound MI359 (PDB id 5FBR, the search space, 34 × 28 × 28, centered at 45.0, 38.0, 53.0, and exhaustiveness 100).

Cell Cultures. HeLa cells were plated onto 35 nm dish with 20 mm glass bottom well (Cellvis, Mountain View, CA). The plasmid DNA was transfected with Extremegene 9 transfection agent (Sigma-Aldrich) according to the manufacturer's protocol. Twenty-four hours after transfection, inhibitor **4** was added to the cell media at 10 nM concentration. After 30 min, the solution was removed, and the cells were immediately imaged in the PBS buffer.

Microscopy. The images of GUVs in the presence of inhibitors were taken on the laser scanning microscope LSM780 (Zeiss, Jena, Germany). The 40×/1.2 water objective lens was used. Compounds **3** and **4** and ATTO647N-DOPE were excited with 405, 490, and 633 nm laser, and the emission light was collected in 433/35, 595/100, and 687/100 bands, respectively.

The FLIM data were collected on external tau-SPAD detectors connected to a FLIM upgrade kit (Picoquant, Berlin, Germany). The excitation of coumarin inhibitor **4** was performed with pulsed 405 nm laser (20 MHz). Simultaneously, iRFP-PI4KB was excited with 633 nm laser. Emission filters 482/35 and 697/58 were used for coumarin and iRFP, respectively.

■ ASSOCIATED CONTENT

Supporting Information

The Supporting Information is available free of charge on the ACS Publications website at DOI: 10.1021/acs.jmedchem.6b01466.

Comparison of fluorescence lifetime images of coumarin-labeled inhibitor (**4**) in HeLa cells expressing only endogenous PI4KB or transiently over-expressing PI4KB-iRFP (PDF)

CSV file with molecular formula strings and the associated biochemical and biological data (CSV)

■ AUTHOR INFORMATION

Corresponding Authors

*E-mail: nencka@uochb.cas.cz (R.N.). Phone: +420-220-183-265.

*E-mail: boura@uochb.cas.cz (E.B.). Phone: +420-220-183-465.

ORCID

Radim Nencka: 0000-0001-6167-0380

Evzen Boura: 0000-0002-9652-4065

Present Address

Institute of Organic Chemistry and Biochemistry, Academy of Sciences of the Czech Republic, v.v.i, Flemingovo nám. 2, 166 10 Prague 6, Czech Republic

Author Contributions

§J.H. and I.M. contributed equally.

Notes

The authors declare no competing financial interest.

■ ACKNOWLEDGMENTS

We are grateful to Eva Zborníková for help with HPLC, to Dominika Chalupska for preparation of the recombinant PI4KB protein, and to Lenka Kloučková for help with bacterial cultures. We are also grateful to Michael Downey for critical reading of the manuscript. The work of I.M., D.C., and R.N. was supported by Czech Science Foundation (Registration No. 15-09310S). The work of E.B. was supported by MarieCurie FP7-PEOPLE-2012-CIG project number 333916. The work was supported by Gilead Sciences, Inc. The project was also supported by the Academy of Sciences of the Czech Republic (RVO 61388963).

■ ABBREVIATIONS

TLC, thin layer chromatography; PI4KB, phosphatidylinositol 4-kinas IIIβ; PI4KA, phosphatidylinositol 4-kinase IIIα; PI4K2A, phosphatidylinositol 4-kinase IIα; PI4P, phosphatidylinositol 4-phosphate; K_D, dissociation constant; HCV, hepatitis C virus; ATP, adenosine triphosphate; ADP, adenosine diphosphate; EtOH, Ethanol; DIPEA, diisopropylethylamine; DCM, dichloromethane; TEA, triisopropylamine; THF, tetrahydrofuran; GUVs, giant unilamellar vesicles; iRFP, near-infrared fluorescent protein; PBS, phosphate-buffered saline; SARS-CoV, severe acute respiratory syndrome coronavirus; FLIM, fluorescence-lifetime imaging microscopy; IC_{50}, half maximal inhibitory concentration; ND, not determined

■ REFERENCES

(1) Rask-Andersen, M.; Almen, M. S.; Schioth, H. B. Trends in the exploitation of novel drug targets. *Nat. Rev. Drug Discovery* **2011**, *10*, 579−590.

(2) Boura, E.; Nencka, R. Phosphatidylinositol 4-kinases: Function, structure, and inhibition. *Exp. Cell Res.* **2015**, *337*, 136−145.

(3) Dornan, G. L.; McPhail, J. A.; Burke, J. E. Type III phosphatidylinositol 4 kinases: structure, function, regulation, signalling and involvement in disease. *Biochem. Soc. Trans.* **2016**, *44*, 260−266.

(4) Minogue, S.; Waugh, M. G. The phosphatidylinositol 4-kinases: don't call it a comeback. *Subcell. Biochem.* **2012**, *58*, 1−24.

(5) Balla, T. Phosphoinositides: Tiny lipids with giant impact on cell regulation. *Physiol. Rev.* **2013**, *93*, 1019−1137.

(6) Tan, J.; Brill, J. A. Cinderella story: PI4P goes from precursor to key signaling molecule. *Crit. Rev. Biochem. Mol. Biol.* **2014**, *49*, 33−58.

(7) Waugh, M. G. PIPs in neurological diseases. *Biochim. Biophys. Acta, Mol. Cell Biol. Lipids* **2015**, *1851*, 1066−1082.

DOI: 10.1021/acs.jmedchem.6b01466
J. Med. Chem. 2017, 60, 119−127

(8) Jovic, M.; Kean, M. J.; Szentpetery, Z.; Polevoy, G.; Gingras, A. C.; Brill, J. A.; Balla, T. Two phosphatidylinositol 4-kinases control lysosomal delivery of the Gaucher disease enzyme, beta-glucocerebrosidase. *Mol. Biol. Cell* **2012**, *23*, 1533−1545.
(9) Jovic, M.; Kean, M. J.; Dubankova, A.; Boura, E.; Gingras, A. C.; Brill, J. A.; Balla, T. Endosomal sorting of VAMP3 is regulated by PI4K2A. *J. Cell Sci.* **2014**, *127*, 3745−3756.
(10) Borawski, J.; Troke, P.; Puyang, X.; Gibaja, V.; Zhao, S.; Mickanin, C.; Leighton-Davies, J.; Wilson, C. J.; Myer, V.; Cornellataracido, I.; Baryza, J.; Tallarico, J.; Joberty, G.; Bantscheff, M.; Schirle, M.; Bouwmeester, T.; Mathy, J. E.; Lin, K.; Compton, T.; Labow, M.; Wiedmann, B.; Gaither, L. A. Class III phosphatidylinositol 4-kinase alpha and beta are novel host factor regulators of hepatitis C virus replication. *J. Virol.* **2009**, *83*, 10058−10074.
(11) Hsu, N. Y.; Ilnytska, O.; Belov, G.; Santiana, M.; Chen, Y. H.; Takvorian, P. M.; Pau, C.; van der Schaar, H.; Kaushik-Basu, N.; Balla, T.; Cameron, C. E.; Ehrenfeld, E.; van Kuppeveld, F. J.; Altan-Bonnet, N. Viral reorganization of the secretory pathway generates distinct organelles for RNA replication. *Cell* **2010**, *141*, 799−811.
(12) Greninger, A. L.; Knudsen, G. M.; Betegon, M.; Burlingame, A. L.; Derisi, J. L. The 3A protein from multiple picornaviruses utilizes the golgi adaptor protein ACBD3 to recruit PI4KIIIbeta. *J. Virol.* **2012**, *86*, 3605−3616.
(13) van der Schaar, H. M.; van der Linden, L.; Lanke, K. H. W.; Strating, J. R. P. M.; Purstinger, G.; de Vries, E.; de Haan, C. A. M.; Neyts, J.; van Kuppeveld, F. J. M. Coxsackievirus mutants that can bypass host factor PI4KIII beta and the need for high levels of PI4P lipids for replication. *Cell Res.* **2012**, *22*, 1576−1592.
(14) Yang, N.; Ma, P.; Lang, J. S.; Zhang, Y. L.; Deng, J. J.; Ju, X. W.; Zhang, G. Y.; Jiang, C. Y. Phosphatidylinositol 4-kinase III beta is required for severe acute respiratory syndrome coronavirus spike-mediated cell entry. *J. Biol. Chem.* **2012**, *287*, 8457−8467.
(15) Spickler, C.; Lippens, J.; Laberge, M. K.; Desmeules, S.; Bellavance, E.; Garneau, M.; Guo, T.; Hucke, O.; Leyssen, P.; Neyts, J.; Vaillancourt, F. H.; Decor, A.; O'Meara, J.; Franti, M.; Gauthier, A. Phosphatidylinositol 4-kinase III beta is essential for replication of human rhinovirus and its inhibition causes a lethal phenotype in vivo. *Antimicrob. Agents Chemother.* **2013**, *57*, 3358−3368.
(16) Altan-Bonnet, N.; Balla, T. Phosphatidylinositol 4-kinases: hostages harnessed to build panviral replication platforms. *Trends Biochem. Sci.* **2012**, *37*, 293−302.
(17) Mejdrova, I.; Chalupska, D.; Kogler, M.; Sala, M.; Plackova, P.; Baumlova, A.; Hrebabecky, H.; Prochazkova, E.; Dejmek, M.; Guillon, R.; Strunin, D.; Weber, J.; Lee, G.; Birkus, G.; Mertlikova-Kaiserova, H.; Boura, E.; Nencka, R. Highly selective phosphatidylinositol 4-kinase IIIbeta inhibitors and structural insight into their mode of action. *J. Med. Chem.* **2015**, *58*, 3767−3793.
(18) Rutaganira, F. U.; Fowler, M. L.; McPhail, J. A.; Gelman, M. A.; Nguyen, K.; Xiong, A.; Dornan, G. L.; Tavshanjian, B.; Glenn, J. S.; Shokat, K. M.; Burke, J. E. Design and structural characterization of potent and selective inhibitors of phosphatidylinositol 4 kinase IIIbeta. *J. Med. Chem.* **2016**, *59*, 1830−1839.
(19) van der Schaar, H. M.; Leyssen, P.; Thibaut, H. J.; de Palma, A.; van der Linden, L.; Lanke, K. H.; Lacroix, C.; Verbeken, E.; Conrath, K.; Macleod, A. M.; Mitchell, D. R.; Palmer, N. J.; van de Poel, H.; Andrews, M.; Neyts, J.; van Kuppeveld, F. J. A novel, broad-spectrum inhibitor of enterovirus replication that targets host cell factor phosphatidylinositol 4-kinase IIIbeta. *Antimicrob. Agents Chemother.* **2013**, *57*, 4971−4981.
(20) Burke, J. E.; Inglis, A. J.; Perisic, O.; Masson, G. R.; McLaughlin, S. H.; Rutaganira, F.; Shokat, K. M.; Williams, R. L. Structures of PI4KIIIbeta complexes show simultaneous recruitment of Rab11 and its effectors. *Science* **2014**, *344*, 1035−1038.
(21) Baumlova, A.; Chalupska, D.; Rozycki, B.; Jovic, M.; Wisniewski, E.; Klima, M.; Dubankova, A.; Kloer, D. P.; Nencka, R.; Balla, T.; Boura, E. The crystal structure of the phosphatidylinositol 4-kinase IIalpha. *EMBO Rep.* **2014**, *15*, 1085−1092.
(22) Klima, M.; Baumlova, A.; Chalupska, D.; Hrebabecky, H.; Dejmek, M.; Nencka, R.; Boura, E. The high-resolution crystal structure of phosphatidylinositol 4-kinase IIbeta and the crystal structure of phosphatidylinositol 4-kinase IIalpha containing a nucleoside analogue provide a structural basis for isoform-specific inhibitor design. *Acta Crystallogr., Sect. D: Biol. Crystallogr.* **2015**, *71*, 1555−1563.
(23) Eisenreichova, A.; Klima, M.; Boura, E. Crystal structures of a yeast 14−3-3 protein from Lachancea thermotolerans in the unliganded form and bound to a human lipid kinase PI4KB-derived peptide reveal high evolutionary conservation. *Acta Crystallogr., Sect. F: Struct. Biol. Commun.* **2016**, *72*, 799−803.
(24) Rozycki, B.; Boura, E. Large, dynamic, multi-protein complexes: a challenge for structural biology. *J. Phys.: Condens. Matter* **2014**, *26*, 463103.
(25) Tai, A. W.; Bojjireddy, N.; Balla, T. A homogeneous and nonisotopic assay for phosphatidylinositol 4-kinases. *Anal. Biochem.* **2011**, *417*, 97−102.
(26) Epps, D. E.; Schostarez, H.; Argoudelis, C. V.; Poorman, R.; Hinzmann, J.; Sawyer, T. K.; Mandel, F. An experimental method for the determination of enzyme-competitive inhibitor dissociation constants from displacement curves: application to human renin using fluorescence energy transfer to a synthetic dansylated inhibitor peptide. *Anal. Biochem.* **1989**, *181*, 172−181.
(27) Wang, X.; Xu, T. Y.; Liu, X. Z.; Zhang, S. L.; Wang, P.; Li, Z. Y.; Guan, Y. F.; Wang, S. N.; Dong, G. Q.; Zhuo, S.; Le, Y. Y.; Sheng, C. Q.; Miao, C. Y. Discovery of novel inhibitors and fluorescent probe targeting NAMPT. *Sci. Rep.* **2015**, *5*, 12657.
(28) Uddin, M. J.; Crews, B. C.; Ghebreselasie, K.; Marnett, L. J. Design, synthesis, and structure-activity relationship studies of fluorescent inhibitors of cycloxygenase-2 as targeted optical imaging agents. *Bioconjugate Chem.* **2013**, *24*, 712−723.
(29) Leriche, G.; Chen, A. C.; Kim, S.; Selkoe, D. J.; Yang, J. Fluorescent analogue of batimastat enables imaging of alpha-secretase in living cells. *ACS Chem. Neurosci.* **2016**, *7*, 40−45.
(30) Zhang, H.; Fan, J.; Wang, K.; Li, J.; Wang, C.; Nie, Y.; Jiang, T.; Mu, H.; Peng, X.; Jiang, K. Highly sensitive naphthalene-based two-photon fluorescent probe for in situ real-time bioimaging of ultratrace cyclooxygenase-2 in living biosystems. *Anal. Chem.* **2014**, *86*, 9131−9138.
(31) MacLeod, A. M.; Mitchell, D. R.; Palmer, N. J.; Van de Poel, H.; Conrath, K.; Andrews, M.; Leyssen, P.; Neyts, J. Identification of a series of compounds with potent antiviral activity for the treatment of enterovirus infections. *ACS Med. Chem. Lett.* **2013**, *4*, 585−589.
(32) Ozers, M. S.; Hill, J. J.; Ervin, K.; Wood, J. R.; Nardulli, A. M.; Royer, C. A.; Gorski, J. Equilibrium binding of estrogen receptor with DNA using fluorescence anisotropy. *J. Biol. Chem.* **1997**, *272*, 30405−30411.
(33) Boura, E.; Silhan, J.; Herman, P.; Vecer, J.; Sulc, M.; Teisinger, J.; Obsilova, V.; Obsil, T. Both the N-terminal loop and wing W2 of the forkhead domain of transcription factor Foxo4 are important for DNA binding. *J. Biol. Chem.* **2007**, *282*, 8265−8275.
(34) Kumar, S.; Rao, V. C.; Rastogi, R. C. Excited-state dipole moments of some hydroxycoumarin dyes using an efficient solvatochromic method based on the solvent polarity parameter, EN(T). *Spectrochim. Acta, Part A* **2001**, *57*, 41−47.
(35) Horng, M. L.; Gardecki, J. A.; Papazyan, A.; Maroncelli, M. Subpicosecond measurements of polar solvation dynamics - coumarin-153 revisited. *J. Phys. Chem.* **1995**, *99*, 17311−17337.
(36) Klima, M.; Toth, D. J.; Hexnerova, R.; Baumlova, A.; Chalupska, D.; Tykvart, J.; Rezabkova, L.; Sengupta, N.; Man, P.; Dubankova, A.; Humpolickova, J.; Nencka, R.; Veverka, V.; Balla, T.; Boura, E. Structural insights and in vitro reconstitution of membrane targeting and activation of human PI4KB by the ACBD3 protein. *Sci. Rep.* **2016**, *6*, 23641.
(37) Nemecek, D.; Boura, E.; Wu, W.; Cheng, N.; Plevka, P.; Qiao, J.; Mindich, L.; Heymann, J. B.; Hurley, J. H.; Steven, A. C. Subunit folds and maturation pathway of a dsRNA virus capsid. *Structure* **2013**, *21*, 1374−1383.
(38) Rezabkova, L.; Boura, E.; Herman, P.; Vecer, J.; Bourova, L.; Sulc, M.; Svoboda, P.; Obsilova, V.; Obsil, T. 14−3-3 protein interacts

DOI: 10.1021/acs.jmedchem.6b01466
J. Med. Chem. 2017, 60, 119−127

with and affects the structure of RGS domain of regulator of G protein signaling 3 (RGS3). *J. Struct. Biol.* **2010**, *170*, 451−461.
(39) Boura, E.; Ivanov, V.; Carlson, L. A.; Mizuuchi, K.; Hurley, J. H. Endosomal sorting complex required for transport (ESCRT) complexes induce phase-separated microdomains in supported lipid bilayers. *J. Biol. Chem.* **2012**, *287*, 28144−28151.
(40) Dejmek, M.; Sala, M.; Hrebabecky, H.; Dracinsky, M.; Prochazkova, E.; Chalupska, D.; Klima, M.; Plackova, P.; Hajek, M.; Andrei, G.; Naesens, L.; Leyssen, P.; Neyts, J.; Balzarini, J.; Boura, E.; Nencka, R. Norbornane-based nucleoside and nucleotide analogues locked in North conformation. *Bioorg. Med. Chem.* **2015**, *23*, 184−191.
(41) Mejdrová, I.; Chalupská, D.; Plačková, P.; Müller, Ch.; Šála, M.; Klíma, M.; Baumlová, A.; Hřebabecký, H.; Procházková, E.; Dejmek, M.; Strunin, D.; Weber, J.; Lee, G.; Mertlíková-Kaiserová, H.; Ziebuhr, J.; Birkus, G.; Boura, E.; Nencka, R.; Matoušová, M. Rational design of novel highly potent and selective phosphatidylinositol 4-kinase IIIβ (PI4KB) inhibitors as broad-spectrum antiviral agents and tools for chemical biology. *J. Med. Chem.* **2016**, DOI: 10.1021/acs.jmedchem.6b01465.

DOI: 10.1021/acs.jmedchem.6b01466
J. Med. Chem. 2017, 60, 119−127